Journal of Power Sources 191 (2009) 669–677

Contents lists available at ScienceDirect

Journal of Power Sources

journal homepage: www.elsevier.com/locate/jpowsour

Poly(vinyl alcohol)/poly(vinyl chloride) composite polymer membranes for secondary zinc electrodes

Chun-Chen Yang[a,*], Jen Ming Yang[b], Cheng-Yeou Wu[c]

[a] Department of Chemical Engineering, Mingchi University of Technology, Taipei Hsien 243, Taiwan, ROC
[b] Department of Chemical and Materials Engineering, Chang Gung University, Kwi-Shan, Tao-Yuan 333, Taiwan, ROC
[c] Taiwan Power Research Institute, Taiwan Power Company, Taipei, Taiwan, ROC

ARTICLE INFO

Article history:
Received 11 June 2008
Received in revised form 16 February 2009
Accepted 17 February 2009
Available online 3 March 2009

Keywords:
PVA
PVC
Microporous
Secondary Zn electrode
Composite polymer membrane
Partial dissolution

ABSTRACT

A microporous composite polymer membrane composed of poly(vinyl alcohol) (PVA) and poly(vinyl chloride) (PVC), was prepared by a solution casting method and a partial dissolution process. The characteristic properties of microporous PVA/PVC composite polymer membranes containing 2.5–10 wt.% PVC polymers as fillers were characterized by thermogravimetric analysis (TGA), X-ray diffraction (XRD), scanning electron microscopy (SEM), capillary flow porometry (CFP), micro-Raman spectroscopy, dynamic mechanical analyzer (DMA) and the AC impedance method. The electrochemical properties of a secondary Zn electrode with the PVA/PVC composite polymer membrane were studied using the galvanostatic charge/discharge method. The PVA/PVC composite polymer membrane showed good thermal, mechanical and electrochemical properties. As a result, the PVA/PVC composite polymer membrane appears to be a good candidate for use on the secondary Zn electrodes.

1. Introduction

The alkaline secondary Zn electrode for Zn–air batteries [1–4] has many advantages such as high specific energy, low cost, and environmentally friendliness. However, the use and development of a secondary Zn electrode [5–10] for rechargeable batteries is still limited due to the dendritic growth, shape change, and the high solubility of zinc discharge products in a concentrated KOH electrolyte. These problems are responsible for the short life-cycle of a secondary Zn electrode and the poor electrochemical performance of the Zn-based batteries. Many attempts have been made to eliminate the Zn dendritic formation, including the use of additives in either the Zn electrode [11,12], or the KOH electrolyte [13–17] as well as in the organic inhibitor or surfactant [18,19]. Yang et al. [9–11] prepared the secondary Zn electrode using calcium zincate as an active material. These calcium zincates ($CaZn_2(OH)_2{\cdot}H_2O$) were prepared by mechanical ball milling of ZnO and $Ca(OH)_2$ in a water medium. Since composite oxides retain lower solubility in a concentrated KOH solution and better charge/discharge reversibility, the problems related to shape changes and dendritic formations can be overcome, thereby enhancing the life-cycle of the secondary Zn electrode. Wang and co-workers [6] also investigated the influence of metallic bismuth powder as an additive and chemically co-precipitated calcium zincate as an active material on the secondary Zn electrodes. Yang et al. [9] studied the electrochemical properties of Ni–Zn batteries with calcium zincates on the secondary Zn electrode by a powder microelectrode technique.

Yang and Lin [20–22] studied and prepared an alkaline polymer electrolyte based on PEO–PVA–KOH to use on the secondary Ni–MH and primary Zn–air batteries. Subramania et al. [23] reported the preparation method for the PVA/PVC porous polymer electrolyte and their applications on a Li-ion battery. Both PVA and PVC polymers were dissolved in the dimethyl formamide (DMF), then formed a homogeneous thin film with a thickness of 150–200 μm. They found the highest ionic conductivity of 1.50×10^{-3} S cm^{-1} with 2 M $LiClO_4$+ EC/DEC (1:1 (v/v)) electrolyte at ambient temperature. A carbon/microporous PVA/PVC electrolyte/$LiMn_2O_4$ cell was assembled and tested.

In the present study, we prepared the composite polymer membrane also using PVA and PVC polymers by a solution cast technique; however, the solvent was water instead of DMF. After the blending, the dried composite PVA/PVC film was also immersed in THF to form a microporous structure through a partial dissolution process [23]. The novel microstructure with a suitable pore size range of 60–180 nm allowed more KOH electrolyte uptake by the PVA/PVC composite polymer membrane ($\sigma \sim 10^{-2}$ S cm^{-1}); however, it also effectively prevented any zinc dendritic formation. Finally, the electrochemical performance of the secondary Zn

* Corresponding author. Tel.: +886 29089899; fax: +886 29041914.
E-mail address: ccyang@mail.mcut.edu.tw (C.-C. Yang).

0378-7753/$ – see front matter © 2009 Elsevier B.V. All rights reserved.
doi:10.1016/j.jpowsour.2009.02.044

electrode based on ball-milled calcium zincates wrapped with the PVA/PVC composite polymer membrane was examined in detail.

2. Experimental

2.1. Preparation of the PVA/PVC composite polymer membranes

PVA (Aldrich), PVC (M.W. 60,000–150,000, Nan-Ya Plastics Corp.) and KOH (Merck) were used as received without further purification. The PVA degree of polymerization and saponification was 1700 and 98–99%, respectively. These microporous PVA/PVC composite polymer electrolyte membranes were prepared using a solution casting method and a partial dissolution process [23]. The appropriate weight ratios of PVA:PVC (=1:0.025–0.10) polymers were dissolved in hot water under stirring. The chemical composition of the PVA polymer was controlled at 10 wt.%. The resulting solution was stirred continuously until the solution mixture took on a homogeneous viscous appearance at 90 °C for 120 min. PVC fillers were added slowly to the mixture in the glass vessel in a slow controlled manner to achieve good distribution of the PVC fillers in the PVA matrix. The PVC fillers did not dissolve in the hot water.

Later, an approximately 5 wt.% gultaldehyde (GA) crosslinker and a 1 vol.% HCl catalyst were added to the above resulting mixture solution, resulting in a mixed polymer solution, which was then poured onto a glass plate. The thickness of the wet composite polymer electrolyte was between 300 and 400 μm. The glass plate containing the viscous PVA/PVC composite polymer membrane was weighed again and then the excess water was allowed to evaporate slowly at a constant temperature of 50 °C at a relative humidity of 30%. Following the water evaporation, the glass plate with the composite polymer membrane was weighed again. The composition of the PVA/PVC composite polymer electrolyte membrane was determined from the mass balance. The thickness of the dried PVA/PVC composite polymer membrane was controlled within the range 150 and 200 μm. Therefore, the microporous PVA/PVC composite polymer membrane was obtained using a partial or preferential dissolution method using THF, which partially dissolved some of the added PVC polymer fillers over 24 h at 25 °C; however, the PVA polymer host was not influenced by THF. Free standing microporous PVA/PVC composite polymer membranes were obtained and packed for further study.

2.2. Thermal, crystal structure, morphology analyses

TGA thermal analysis was carried out using a Mettler Toledo TGA/SDT 851^e system. Measurements were taken after heating from 30 to 600 °C under N_2 atmosphere at a heating rate of 10 °C min^{-1} with a sample of about 10 mg. The crystal structures of the PVA/PVC composite polymer membranes were examined using a Philips X'Pert X-ray diffractometer (XRD) with Cu Kα radiation of wavelength λ = 1.54056 Å for 2θ angles between 10 and 90°. The surface morphology and microstructure of the PVA/PVC composite polymer membranes was examined using an S-2600H scanning electron microscopy (SEM) (Hitachi Co., Ltd.).

2.3. Analysis of mean pore size and pore size distribution

Capillary flow porometry (PMI, CFP-1200-AE, USA) was used to measure the mean pore size and the pore size distribution. For comparison, two commercial separators, including a PP/PE separator (Coin) and a PE separator (Celgard 5550), were also examined. These separators and the PVA/PVC composite polymer membranes were first soaked with a wetting agent (a Porewick with a surface tension of 16 dyn cm^{-1}), and then N_2 gas was applied to one side of the composite polymer membranes and the separators. The N_2 gas pressure (0–200 psi) was increased slowly until the Porewick liquid was removed from the pores and a gas flow formed. The gas flow rate as a function of pressure was measured and used to calculate the diameter of each pore, the mean flow pore diameter and the pore size distribution data. The experimental setup and measurement methods have previously been described in detail [24–26].

2.4. Mechanical properties and micro-Raman spectroscopy analyses

Dynamic mechanical analyses (DMA) were conducted using a RSA-III Instrument dynamic mechanical analyzer (TA) at a frequency of 1 Hz and oscillation amplitude of 0.15 mm. The temperature range studied was from 25 to 150 °C with a heating rate of 5 °C min^{-1}. The micro-Raman analysis was carried out using a Renishaw confocal microscopy Raman spectroscopy system, including a microscope equipped with a 50× objective and a charge-coupled device (CCD) detector. The Raman excitation source was provided by a 633 nm laser beam, which had a beam power of 10 mW that was focused on a spot of about 1 μm in diameter.

2.5. The ionic conductivity measurements, liquid absorption and swelling ratios

The conductivity measurements for the alkaline PVA/PVC composite polymer membrane were measured by the AC impedance method [20–22]. The samples of the PVA/PVC composite polymer membranes were immersed in a 8 M KOH solution for at least 24 h before the test. These alkaline PVA/PVC composite polymer electrolytes were sandwiched between SS304 stainless steel and ion-blocking electrodes, each of surface area 1.32 cm^2, in a spring-loaded glass holder. A thermocouple was kept in close to the composite polymer electrolytes to allow for temperature measurements. Each sample was equilibrated at the experimental temperature for at least 60 min before the measurement was taken. AC impedance measurements were carried out using Autolab PGSTAT-30 equipment (Eco Chemie B.V., The Netherlands). The AC frequency ranged from 100 kHz to 10 Hz at an excitation signal of 5 mV. The AC impedance of the PVA/PVC composite polymer electrolyte was recorded within a temperature range of 30–70 °C. Experimental temperatures were maintained within ±0.2 °C using a convection oven. All alkaline PVA/PVC composite polymer electrolytes were examined at least three times.

The pre-weighed, dried PVA/PVC composite polymer membrane (W_o) was immersed in distilled water, and maintained for 24 h at 25 °C. The PVA/PVC composite polymer membrane was then removed from the immersion bath and the excess surface water was carefully removed. The weight of the wet composite polymer membrane (W_1) was then determined again. The absorption percentages of H_2O and the swelling ratio were calculated from the following equations [20–22]:

$$\text{Liquid absorption}\,(\%) = \frac{W_1 - W_o}{W_1} \times 100 \quad (1)$$

$$\text{Swelling ratio}\,(\%) = \frac{W_1 - W_o}{W_o} \times 100 \quad (2)$$

2.6. Preparation of a secondary Zn electrode and the property measurements

Calcium zincate powder was prepared using a mechanical ball-milled powder consisting of ZnO (Aldrich) and $Ca(OH)_2$ (Aldrich) with the mole ratio of Zn:Ca = 2.5:1. A suitable amount of powdered ZnO and $Ca(OH)_2$ was weighed, mixed and put into an agate pot with a 10 mm in diameter agate ball. The weight ratio of the active materials to the mill ball was set at 1:5. The ball-milled pot was

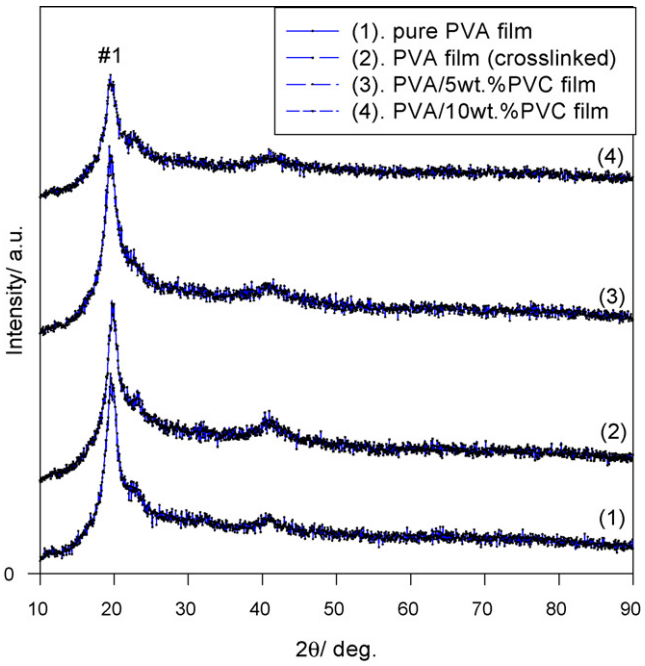

Fig. 1. XRD spectra for the PVA/PVC composite polymer membranes with various amounts of PVC fillers.

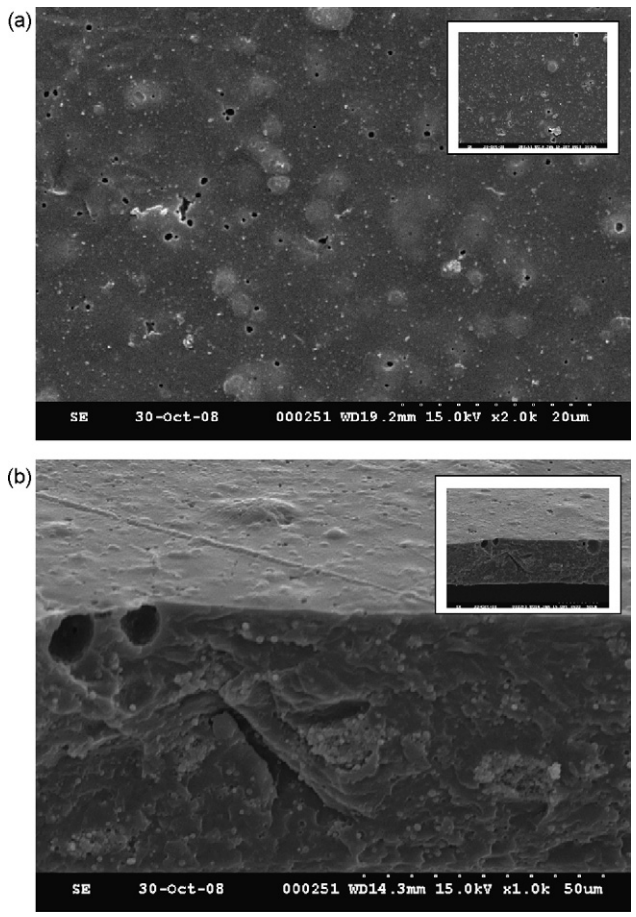

Fig. 2. SEM photographs of the PVA/10 wt.% PVC composite polymer membrane: (a) top view at 2k× and at 400× for the inset; (b) the cross-sectional views at 1k× and at 500× for the inset.

tightly sealed and set in a planetary ball miller (FRITSCH 7). The mechanical ball mill rotated at a speed of 300 rpm for 12 h at ambient temperature, following which the Zn working electrode based on a mixture of calcium zincate slurry was prepared.

The slurry pastes for the secondary Zn electrodes were prepared as follows: we mixed 70 wt.% ball-milled calcium zincate powders, 8 wt.% Zn powders (Aldrich), 2 wt.% Cu powders (Aldrich), 2 wt.% PbO (Aldrich), 3 wt.% Bi_2O_3 (Aldrich) and 15 wt.% PTFE (30J, DuPont) binder solution. In order to enhance the cycleability and utilization of the secondary Zn electrodes, 2 wt.% of Cu conductive nanopowders were added to the mixture slurry. A large section (5 cm × 5 cm) of Pt sheet was used as a counter electrode and a Hg/HgO electrode was used as a reference electrode. The galvonostatic charge/discharge measurements were carried out on the secondary Zn electrode ($A = 4\,cm^2$) wrapped with the PVA/PVC composite polymer membrane at a C/10 charge rate and a C/5 discharge rate. All electrode potentials were recorded vs. a $Hg/HgO/OH^-$. The electrolyte was a ZnO saturated 8 M KOH aqueous solution.

3. Results and discussion

3.1. Crystal structure and surface morphology

An X-ray diffraction measurement was performed to examine the nature of the crystallinity of the PVA/PVC composite polymer membranes. Fig. 1 shows the diffraction pattern for the PVA polymer film and the PVA/PVC composite polymer membranes. It is well known that the PVA polymer film exhibits a semi-crystalline structure with peaks at the 2θ angles of 20° and 40°. As can be seen clearly in Fig. 1, a large peak of 20° at 2θ (i.e., peak#1) for the PVA polymer film occurred. But, the peak intensities of the PVA/PVC composite polymer membranes were decreased as the PVC fillers were added. This implies that the addition of the PVC fillers into the PVA polymer matrix greatly augmented the domain of the amorphous region (i.e., the intensity of the XRD crystal peak decreased).

XRD results also indicated that the PVA/PVC composite polymer membrane became more amorphous, which were supported by the decrease of the relative crystallinity of the PVA/PVC composite polymer membranes from 64% to 41%, as displayed in Table 1. Note that the degree of amorphousness was increased the amount of PVC fillers was increased. Either a significant motion of polymer chain in the amorphous domains existed, or some defects and free volumes existed at the interface between the polymer chains during non-conducting in the crystalline phases. The characteris-

Table 1
The percents of crystallinity of the microporous PVA/PVC composite polymer membranes.

Types	2θ (°)				
	Peak#1 position	Intensity#1	Peak#2 position	Intensity#1	Relative crystallinity (%)[a]
PVA film	19.53°	1104	39.83°	603	100
PVA (crosslinked)	19.68°	954	40.32°	568	86
PVA/5 wt.% PVC	19.38°	707	41.47°	238	64
PVA/10 wt.% PVC	19.53°	460	40.87°	198	41

[a] Based on peak#1 of XRD result.

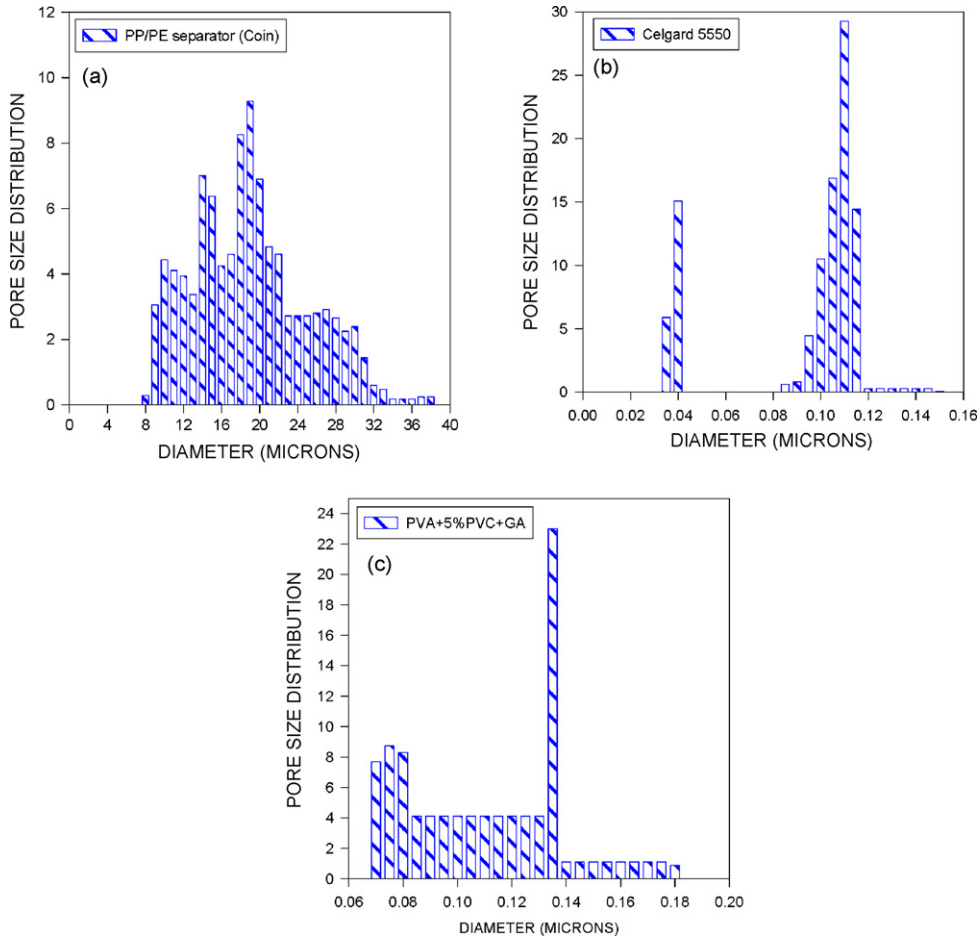

Fig. 3. The pore size distribution curves for: (a) PP/PE separator (Coin); (b) the PE separator (Celgard 5550); (c) the PVA/5 wt.% PVC polymer membrane.

tics of the PVA/PVC composite polymer membranes showed good ionic conductivity property due to the formation of more amorphous domains facilitating the local PVA chain segmental motion in the PVA/PVC composite polymer membrane (as seen in Section 3.4).

Fig. 2(a) shows SEM photographs of the top view of PVA/10 wt.% PVC composite polymer membranes at 1k× and at 400× for the inset. It was observed that the surface morphology of the PVA/PVC composite polymer membrane showed good uniformity and the added PVA fillers were well-dispersed into the PVA polymer host. Further, the SEM photographs for the cross-sectional view of the PVA/PVC composite polymer membrane are shown in Fig. 2(b) at 1k× and at 500× for the inset. The micropores size of the PVA/PVC composite polymer membranes were about 0.1–0.2 μm (the PVA filler size about 100–200 nm) with a spherical shape. Some large voids or big pores (those formed from PVC aggregates) was found about 2–10 μm, as shown in Fig. 2(b). After the preferential dissolution treatment in Tetrahydrofuran (THF) for 24 h, some PVC fillers were partially dissolved away at room temperature and the microporous structure of the PVA/PVC composite polymer membrane was then obtained. It was found that the weight losses of the PVA polymer film and the PVA/5 wt.% PVC composite polymer film in a THF solvent at 25 °C for 24 h were 0.15–0.23% and 0.70–1.10%, respectively. It was calculated about 15–20 wt.% PVC polymer being dissolved, especially near the top and bottom surfaces of the polymer membranes. Importantly, the composition of the PVC fillers, the size of the PVC *fillers*, the immersion time, and the dissolution temperature were crucial in terms of controlling the porous size and the pore size distribution in the PVA/PVC composite polymer membrane. Generally, the PVA/PVC composite polymer membranes proved to be compatible and homogenous. Moreover, it is particularly worthy to note that the amount of the added PVC fillers needed to be less than 20 wt.% in order to obtain a well-dispersed composite polymer membrane.

The microstructures of the PVA/PVC composite polymer membrane with an optimal pore size (i.e., in the range of 60–120 nm) can help retain more KOH electrolyte and also effectively prevent the formation of dendritic Zn deposits during the charge period.

3.2. Pore size and pore size distribution

The structural and porosity properties of the polymer separators or the microporous composite polymer membrane are extremely important for the secondary Zn electrode. Shape change and the dendritic formation of a secondary Zn electrode during the charge/discharge process were the most common problems, which can be solved by using the polymer separator or the composite polymer membrane with the suitable pore size and pore size distribution. A novel method based on capillary flow porometry (CFP) was used to examine the microporous characteristic property of the PVA/PVC composite polymer membrane. In particular, this technique measures go-through pores in the polymer membrane, but not the blind pores. Moreover, the capillary flow porometer can also effectively examine the micropore structure of porous materials or membranes consisting of several layers in any direction (in plane and through plane) [24–26]. Fig. 3(a–c) shows the pore size distribution for two battery separators (i.e., Coin's PP/PE and Celgard's PE) and the PVA/5 wt.% PVC composite polymer membrane,

Table 2
The pore sizes and pore size distributions for two battery separators and the PVA/PVC composite polymer membranes.

Types	Diameter (μm)			
	Largest pore	Mean flow pore	Smallest pore	At maximum pore distribution
PP/PE separator	43.75	18.05	6.58	19.00
PE separator	0.151	0.108	0.037	0.110
PVA/5 wt.% PVC	0.179	0.110	0.066	0.135
PVA/10 wt.% PVC	0.182	0.115	0.062	0.100

respectively. For comparison, Fig. 3(a and b) present the pore size distributions for two commercially separators, whereas the first one is a Coin's PP/PE separator and the other is a Celgard's PE separator. The experimental results indicated that the mean pore size of the PP/PE separator was around 18.05 μm, which is close to the specification of 20 μm. These PP/PE separators with very large pore size of 18–20 μm are not suitable for the secondary Zn electrode application; it will cause the formation of dendritic Zn deposits. In addition, the PP/PE separator not retained much KOH electrolyte; it showed lower ionic conductivity.

Moreover, the experimental results also showed that the mean pore size of the PE separator (Celgard) was around 108 nm, which is close to the product specification around 100 nm. Although Celgard separator showed excellent chemical and mechanical properties to prevent the shape change for the Zn electrode, it also showed poor performance for the life-cycle of the secondary Zn electrode, it was due to the formation of dendritic Zn deposits.

In addition, it was observed that the mean pore diameters of the PVA/PVC composite membranes with the composition of 5 and 10 wt.% PVC fillers were around 110 nm and 115 nm, respectively. However, the mean pore size of the pure PVA membrane was less than 30 nm, which the pores size of the pure PVA membrane was indeed much smaller than that of the PVA/PVC composite membranes.

Table 2 shows the test results for the largest pore, the mean flow pore, the smallest detected pore, and at the maximum pore distribution for all samples including two separators and the PVA/PVC composite polymer membranes.

Interestingly, the pore size distributions of the PVA/PVC composite polymer membranes and the PE separator (Celgard), were in the range of 40–180 nm. By comparison, the mean pore size of the PVA/PVC composite polymer membranes (ca. 110–115 nm) was close to that of the PE separator (ca. 108 nm).

3.3. TGA thermal analysis

TGA thermographs of PVC powders, pure PVA film, gultaldehyde solution (25 wt.%), and the PVA/5 wt.% PVC composite polymer membrane are shown in Fig. 4(a), respectively. Clearly, the weight loss of the PVA/PVC + GA composite polymer membrane was much less as compared with the pure PVA+GA film within the temperature range of 100–300 °C. However, the PVC polymers started degrading at around 300 °C, as shown in Fig. 4(a). It can be seen that the thermal stability of the PVA/PVC composite polymer membrane improved greatly when the PVC fillers were added.

Moreover, the TGA thermographs of these PVA/PVC composite polymer membranes containing 0.2–10 wt.% of PVC fillers are shown in Fig. 4(b). There was a weight loss of 0.63% at a temperature of 100 °C for the pure PVA polymer film (without PVC fillers); this was due to the removal of some bounding water. In contrast, all PVA/PVC composite polymer membranes underwent a four-step degradation (shown as $T_{d,1}$ = 100 °C, $T_{d,2}$ = 275 °C, $T_{d,3}$ = 375 °C, $T_{d,4}$ = 430 °C), which began in the region between 90 and 100 °C, leading to a weight of loss of 3–4%. There was a thermal stable region

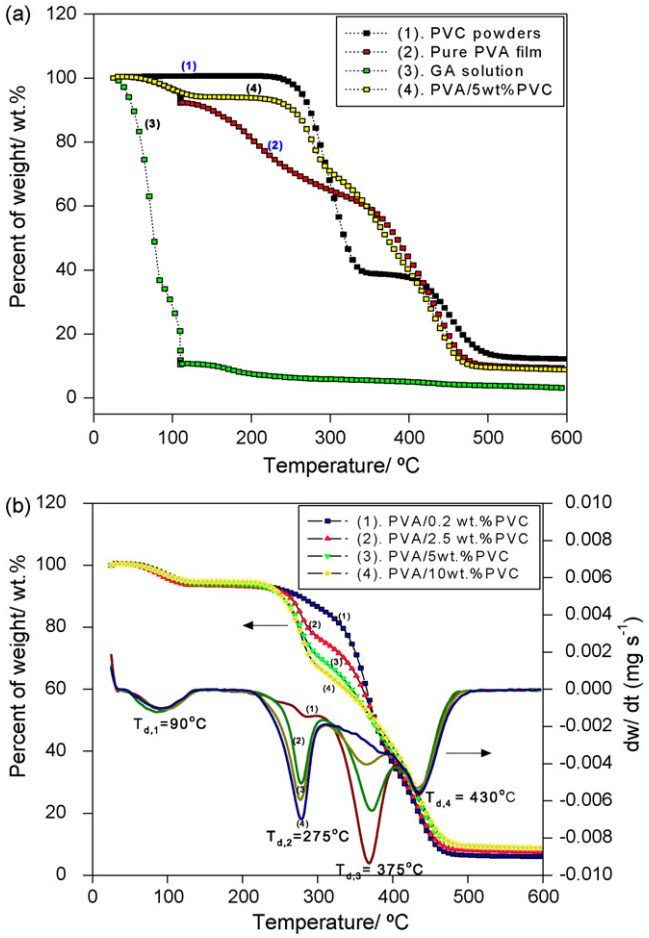

Fig. 4. TGA thermographs: (a) PVA, PVC, GA, and PVA/5 wt.% PVC composite membrane; (b) PVA/PVC composite polymer membranes with various compositions.

between 100 and 250 °C. Subsequently, there was a 7–10% weight loss when the temperature reached approximately 250 °C; there was a 29–43% weight loss when the temperature reached between 250 and 350 °C. This stage showed a significant weight loss, the composite polymer membranes started to decompose. Finally there was a total weight loss of 91–92% when the temperature was greater than 480 °C.

In conclusion, the PVA/PVC + GA composite polymer membrane started to degrade at 250 °C; however, the pure PVA + GA polymer film (without PVC fillers) gradually degraded after 150 °C. It is clear that the addition of the PVC fillers markedly improved the thermal stability of the PVA/PVC polymer membranes. Table 3 shows the detailed weight loss results for these PVA/PVC composite polymer membranes with various compositions at different temperatures by TGA analysis.

3.4. Ionic conductivities, liquid uptake and swelling ratio

A typical AC impedance spectrum of the alkaline PVA/PVC composite polymer electrolyte membranes with 5 wt.% PVC fillers at different temperatures is shown in Fig. 5. The AC spectrum were typically non-vertical spikes for blocking electrodes, i.e., SS |PVA/PVC SPE| SS cell. Analysis of the spectrum yielded information about the properties of the PVA/PVC composite polymer membrane, such as bulk resistance (R_b). Taking into account the thickness of the composite polymer electrolyte film, the R_b value was converted into the ionic conductivity, σ, according to the for-

Table 3
The weight loss of the PVA/PVC composite polymer membranes at various temperatures.

Types	%			
	Temperature (100 °C)	Temperature (250 °C)	Temperature (350 °C)	Temperature (600 °C)
PVC powders	0.60	1.93	61.08	87.80
PVA film (crosslinked)	0.63	8.00	73.10	92.24
PVA/0.2 wt.% PVC	3.27	7.09	28.90	93.98
PVA/2.5 wt.% PVC	4.45	8.69	35.74	92.53
PVA/5 wt.% PVC	3.53	9.98	42.05	91.13
PVA/10 wt.% PVC	3.34	10.00	43.41	91.21

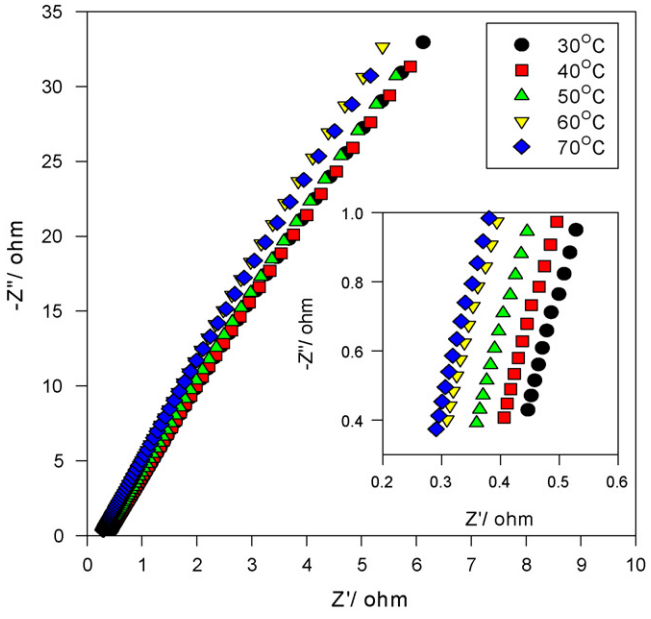

Fig. 5. Nyquist plot of alkaline PVA/5 wt.% PVC composite polymer electrolyte.

mula [20–22]:

$$\sigma = \frac{L}{R_b A} \tag{3}$$

where L is the thickness (cm) of the composite polymer electrolyte, A is the area of the blocking electrode (cm^2), and R_b is the bulk resistance (ohm) of alkaline PVA/PVC composite polymer electrolyte.

Typically, the R_b values of the PVA/5 wt.% PVC composite polymer electrolytes were in the order of 0.25–0.45 Ω and were highly dependent on the temperature, as shown in the inset of Fig. 5. The corresponding value of the ionic conductivity at ambient temperature is 0.0251 S cm^{-1}. The AC impedance spectrum of the PVA/10 wt.% PVC composite polymer membrane (σ = 0.0371 S cm^{-1} at 30 °C) was also obtained (not shown here).

Table 4 shows the ionic conductivity values for all PVA/PVC composite polymer membranes with various PVC compositions, i.e., 2.5, 5 and 10 wt.%. It was observed that the highest ionic conductivity value (σ = 0.0371 S cm^{-1} at 30 °C) was for PVA/10 wt.% PVC composite polymer electrolyte, leading to the conclusion that the ionic conductivity of the PVA/PVC composite polymer electrolytes can be increased when a suitable amount of the PVC fillers was added. This may be due to the higher portion of amorphous domain in the PVA/PVC composite polymer electrolyte when the PVC fillers were used as the solid plasticizer. The ion conduction mechanism for alkaline PVA/PVC composite polymer electrolyte is mainly due to the OH^- ion as a carrier ($t^- \sim 1$). It is because the hydrophilic PVA polymers have the side chain of the hydroxide (–OH) group; they can retain more KOH electrolyte. Additionally, the crystallinity of the PVA polymer was reduced as the PVC fillers was added; it will augment amorphous domain in the PVA polymer matrix. It was well known that the ion conduction occurred only in the amorphous region of the composite polymer electrolyte [20–22]. Moreover, these microstructures also allow more KOH electrolyte to retain at the interface, which is like a micro-reservoir; it can effectively enhance mass transport rate for these charge carriers.

The temperature dependence of the ionic conductivity is of the Arrhenius type:

$$\sigma = \sigma_o \exp\left(-\frac{E_a}{RT}\right) \tag{4}$$

where σ_o is a pre-exponential factor, E_a is the activation energy, and T is the temperature in Kelvins. The $\log_{10}(\sigma)$ vs. $1/T$ plots (not shown here) obtains the activation energy (E_a) of the PVA/PVC composite polymer electrolytes, which is dependent on the composition of the PVA/PVC composite polymer electrolyte. The E_a value of the PVA/PVC composite polymer electrolytes was of the order of 9–12 kJ mol^{-1}. The activation energy (E_a) for alkaline PVA–KOH–H_2O polymer electrolyte was found in the order of 3–15 kJ mol^{-1} [21,22]; however, Lewandowski et al. [27] showed the E_a value of 22–28 kJ mol^{-1} and the ionic conductivity of 10^{-3} S cm^{-1} for alkaline PVA–KOH–H_2O solid electrolytes with the chemical composition of 40 wt.% PVA, 24–39 wt.% KOH, and 30–35 wt.% H_2O. It is well-accepted that the lower the value of E_a is, the faster is the ion conduction in the composite polymer electrolyte [20–22].

Further, the dimension stability of the PVA/PVC composite polymer membrane is also very important for a practical application. The results of the absorption percent (%) and swelling ratio for the PVA/PVC composite polymer membrane in D.I. water are shown in Table 5. It was found that the absorption percent of D.I. water for the PVA/PVC composite polymer membranes decreased from 52% to 44% when the amount of the PVC fillers increased from 2.5 to 10 wt.%. Furthermore, the swelling ratio for the PVA/PVC composite polymer membranes in D.I. water decreased from 119% to 87% when the amount of the PVC fillers increased from 2.5 to 10 wt.%. As

Table 4
The ionic conductivities of alkaline PVA/PVC composite polymer electrolytes with various amounts of PVC fillers.

Types	σ(S cm^{-1})				
	30 °C	40 °C	50 °C	60 °C	70 °C
PVA/2.5 wt.% PVC	0.0120	0.0169	0.0197	0.0222	0.0247
PVA/5 wt.% PVC	0.0251	0.0272	0.0295	0.0315	0.0335
PVA/10 wt.% PVC	0.0371	0.0407	0.0451	0.0487	0.0520

Table 5
The results of D.I. water absorption and swelling ratio of microporous PVA/PVC composite polymer membranes with various amounts of PVC fillers.

Types	Parameters		
	Thickness (μm)	Absorption (%)	Swelling ratio (%)
PVA/0.2 wt.% PVC	109	52	119
PVA/2.5 wt.% PVC	188	51	108
PVA/5 wt.% PVC	174	47	90
PVA/10 wt.% PVC	166	44	87

we know, when the PVC filler used as a stiffer material was added to the soft PVA matrix, the swelling ratio of the PVA/PVC composite polymer membrane was greatly reduced. Thus, the dimension stability is markedly improved.

3.5. Micro-Raman spectroscopy and DMA analyses

Fig. 6(a) shows the variation of storage modulus (E') with temperature for pure PVA film and PVA/PVC composite polymer membranes up to 20 wt.% PVC fillers. The storage modulus of the pure PVA ($E' = 7.68 \times 10^8$ Pa) film was lower than those of the PVA/5–20 wt.% PVC composite polymer membranes ($E' = 2.82$–3.86×10^9 Pa) at 25 °C. It was clear that the storage moduli of the PVA/5–20 wt.% PVC composite polymer membranes increased with increasing the loading of PVC fillers. It also confirmed that the added PVC fillers enhanced the mechanical properties of the PVA/PVC composite polymer membranes. However, when the amount of the PVC fillers was 20 wt.%, the stiffening effect was progressively reduced due to the agglomeration of the PVC fillers within the PVA polymer host, as shown in Fig. 6(a).

Fig. 6(b) shows the loss factor or tan (δ) vs. temperature for the pure PVA and PVC films, and these PVA/PVC composite polymer membranes. The glass transition temperatures (T_g) can be taken at the peak of tan (δ) curves. The results indicated that the glass transition temperatures of pure PVA film ($T_{g,PVA}$) and pure PVC film ($T_{g,PVC}$) were 47.4 °C and 88.7 °C, respectively. Apparently, it was found that there were three tan δ peaks for all PVA/PVC composite polymer membranes; the first tan (δ) peak ($T_{p1,PVA}$) was located at between 50 and 52 °C; however, the secondary tan (δ) peak ($T_{p2,PVC}$) was found at between 78 and 81 °C. The broad and decrease of these tan (δ) peaks of PVA/PVC composite polymer membranes can be described as the incompatibility for those two polymer materials. The third tan (δ) peak ($T_{p3,PVA}$) at 116–123 °C may be due to the slip of the PVA molecular chains containing some chemically bonded water [28].

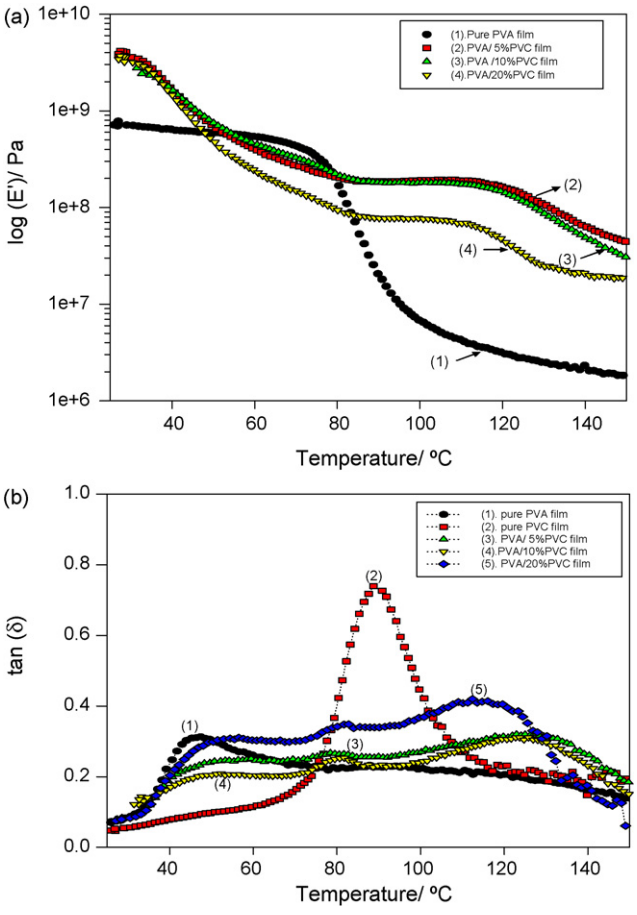

Fig. 6. The curves of storage modulus (a); and loss factor (b) vs. temperature for the PVA/PVC composite polymer membranes.

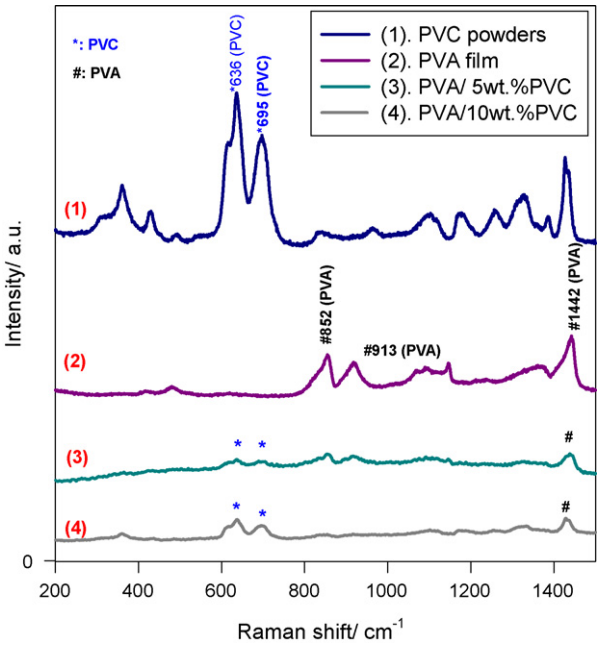

Fig. 7. Micro-Raman spectra of PVC powders, PVA film and these PVA/PVC composite polymer membranes.

Fig. 7 shows the micro-Raman spectra of the PVC powders, pure PVA film (crosslinked) and the PVA/5–10 wt.% PVC composite polymer membranes. It can be seen clearly from the micro-Raman spectra that two strong characteristic scattering peaks at 636 and 695 cm^{-1}, which were related to the PVC filler; they were due to the C—Cl stretching vibration [29]. By contrast, there was also a strong vibration peak at 1442 cm^{-1}, which was assigned to the C—H bending and O—H bending of PVA polymer [30]. Moreover, there were also two weak micro-Raman scattering peaks for the PVA polymer at 852 and 913 cm^{-1}, which may have resulted from the C—C stretching. Finally, there were several weak scattering peaks at 1145 and 1088 cm^{-1}, which were due to the C—C stretching and the C—O stretching. On the whole, it can be seen that the intensities of these characteristic vibrational peaks for the PVA/PVC composite polymer membranes were decreased; it indicated that the amorphous domains in the PVA matrix were augmented.

3.6. The galvanostatic charge/discharge measurements

Fig. 8(a and b) shows the charge/discharge potential (E–t) curves of the secondary Zn electrode wrapped with the PVA/10 wt.% PVC composite polymer membrane and the PE (Celgard) separator, respectively, at a charge rate of C/10 and a discharge rate of C/5 at 1–5 cycles after the formation process. It was found that the charge potential of the secondary Zn electrode with PVA/PVC composite polymer membrane was much smooth and stable. This may result from the unique microporous structure for the PVA/PVC composite polymer membrane. The possibility for the formation of dendritic Zn deposits or the shape change was greatly reduced by using microporous PVA/PVC composite polymer membrane during the overcharge period. More importantly, the life-cycle of the secondary Zn electrode was greatly extended. In fact, the charge potential of the secondary Zn electrode with the PVA/PVC composite poly-

mer membrane was very stable and it varies at between −1.40 and −1.45 V (vs. Hg/HgO). It may be due to the high ionic conductivity and unique microporous structure of the PVA/PVC composite polymer electrolyte membrane. As a result, the Zn electrode potential during the charge period was much less polarized; therefore, the current efficiency and the life-cycle of the Zn electrode were effectively improved. By contrast, it was shown that the charge potential of the secondary Zn electrode with a PE separator was not smooth and unstable, as shown in Fig. 8(b). It may be due to the poor compatibility of the PE separator and the secondary Zn electrode.

Fig. 9 shows the specific discharge capacity vs. the number of cycles curves for the secondary Zn electrode wrapped with the PVA/10 wt.% PVC composite polymer membrane at C/5 rate. It was found that the mean specific discharge capacity (Q_{avg}) of the secondary Zn electrode based on the ball-milled ZnO + $Ca(OH)_2$ powders was approximately 353 mAh g_{ZnCa}^{-1} for 45 cycles (theoretical ZnO specific capacity is 658.8 mAh g_{ZnO}^{-1}; however, the theoretical capacity of ball-milled ZnCa active materials with a mole ratio of Zn:Ca = 2.5:1 is 529 mAh g_{ZnCa}^{-1}. It was discovered that the current efficiency (ratio of the discharge capacity to the charge quantity of electricity) was about 70–80% and the percent of utilization of our lab-made ZnCa active materials was approximately 65–75%. It was demonstrated that the discharge capacity of a secondary Zn electrode was improved by utilizing the microporous PVA/PVC composite polymer membrane (Q_{avg} = 353 mAh g_{ZnCa}^{-1}), as compared with the PE separator (Q_{avg} = 250 mAh g_{ZnCa}^{-1}). Besides, the pore size and pore size distribution of the PVA/PVC composite polymer membrane could be systematically designed and controlled by a suitable amount of the PVC fillers, the partial dissolution time and the etching temperature.

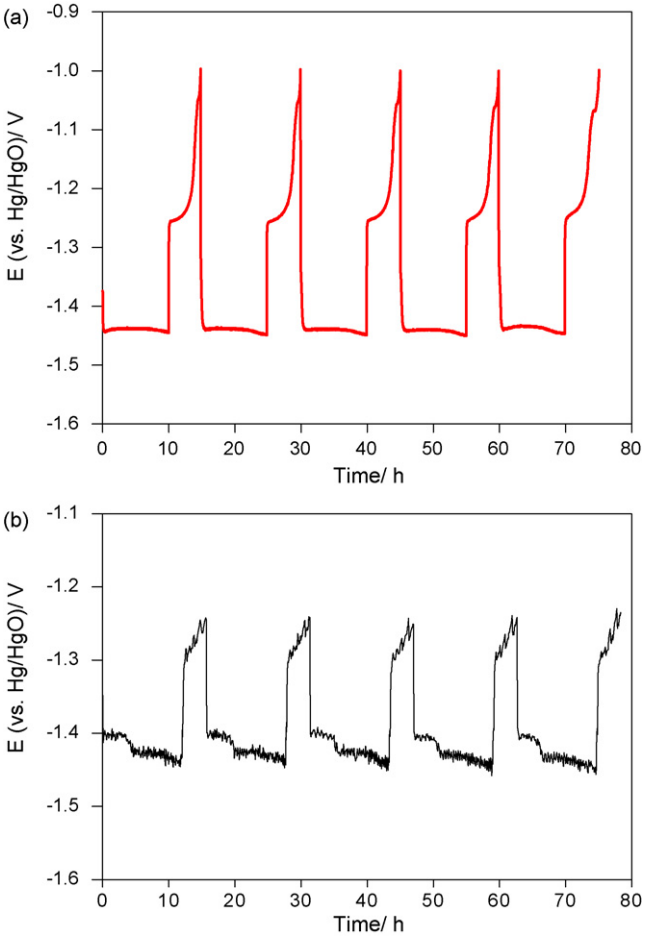

Fig. 8. The *E*–*t* curves of the secondary Zn electrodes wrapped with: (a) PVA/10 wt.% PVC membrane; (b) the PE separator at the C/10 charge and C/5 discharge rates.

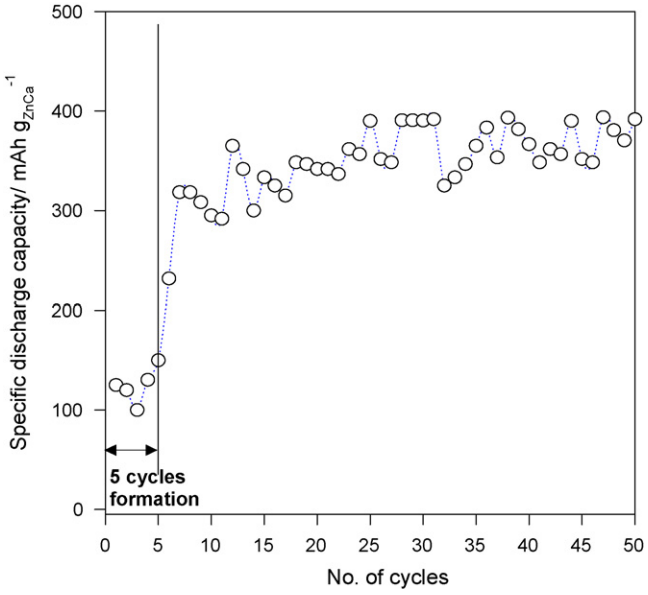

Fig. 9. The specific discharge capacity vs. the number of cycles for the secondary Zn electrode wrapped with the PVA/10 wt.% PVC composite polymer membrane.

4. Conclusions

A microporous PVA/PVC composite polymer membrane was prepared and examined. The characteristic properties of the PVA/PVC composite polymer membranes were systematically examined by using XRD, SEM, TGA, capillary flow porometry, micro-Raman spectroscopy, dynamic mechanical analysis and the AC impedance method. It was found that CFP proved a very useful tool to characterize the micropore properties of the PVA/PVC composite polymer membrane. TGA result indicated that the thermal and mechanical properties of the PVA/PVC composite polymer membranes were enhanced when the PVC fillers were added. The galvanostatic charge/discharge tests were conducted on the secondary Zn electrode. The life-cycle of the secondary Zn electrode wrapped with the microporous PVA/PVC composite polymer membrane was extended over 50 cycles. At the present time, only few polymer electrolyte membranes are commercially available for the Zn-based batteries, such as Ni–Zn or Zn–air cells. The PVA/PVC composite polymer membrane appears to be a good candidate for use on the secondary Zn-based batteries.

Acknowledgement

Financial support from the Taiwan Power Company, Taiwan (Project No: TPC-546-4311-9401B) is gratefully acknowledged.

References

[1] J.W. Evans, G. Savaskan, J. Appl. Electrochem. 21 (1991) 105–110.
[2] G. Savaskan, T. Huh, J.W. Evans, J. Appl. Electrochem. 22 (1992) 909–915.
[3] T. Huh, G. Savaskan, J.W. Evans, J. Appl. Electrochem. 22 (1992) 916–921.
[4] J.C. Salas-Morales, J.W. Evans, J. Appl. Electrochem. 24 (1994) 858–862.
[5] X.M. Zhu, H.-X. Yang, X.-P. Ai, J.-X. Yu, Y.-L. Cao, J. Appl. Electrochem. 33 (2003) 607–612.
[6] C. Zhang, J.M. Wang, L. Zhang, C.N. Cao, J. Appl. Electrochem. 31 (2001) 1049–1054.
[7] S. Muller, F. Holzer, O. Haas, J. Appl. Electrochem. 28 (1998) 895–898.
[8] C. Zhang, J.M. Wang, H. Chen, J.Q. Zhang, C.N. Cao, Mater. Chem. Phys. 84 (2004) 99–106.

[9] H. Yang, H. Zhang, X. Wang, J. Wang, X. Meng, Z. Zhou, J. Electrochem. Soc. 151 (2004) A2126–A2131.
[10] J. Yu, H. Yang, X. Ai, X. Zhu, J. Power Sources 103 (2001) 93–97.
[11] H. Yang, X. Meng, E. Yang, X. Wang, Z. Zhou, J. Electrochem. Soc. 151 (2004) A389–A393.
[12] M. Geng, D.O. Northwood, Int. J. Hydrogen Energy 28 (2003) 633–636.
[13] Y. Ein-Eli, M. Auinat, D. Starsvetsky, J. Power Sources 114 (2003) 330–337.
[14] Y. Ein-Eli, Electrochem. Solid-State Lett. 7 (No. 1) (2004) B5–B7.
[15] Y. Ein-Eli, M. Auinat, J. Electrochem. Soc. 150 (No. 12) (2003) A1606–A1613.
[16] Y. Ein-Eli, M. Auinat, J. Electrochem. Soc. 150 (No. 12) (2003) A1614–A1622.
[17] Y. Ein-Eli, M. Auinat, Y. Zingerman, U.S. Patent 6,544,686 (2003).
[18] J. Dobryszycki, S. Biallozor, Corros. Sci. 43 (2001) 1309–1319.
[19] H. Yang, Y. Cao, X. Ai, L. Xiao, J. Power Sources 128 (2004) 97–101.
[20] C.C. Yang, S.J. Lin, J. Power Sources 112 (2002) 497–503.
[21] C.C. Yang, Mater. Lett. 57 (2002) 873–881.
[22] C.C. Yang, S.J. Lin, J. Appl. Electrochem. 33 (2003) 777–784.
[23] A. Subramania, N.T. Kalyyana Sundaram, N. Sukumar, J. Power Sources 141 (2005) 188–192.
[24] A. Jena, K. Gupta, J. Power Sources 96 (2001) 214–219.
[25] A. Gigova, J. Power Sources 158 (2006) 1054–1061.
[26] J.P. Feser, A.K. Prasad, S.G. Advani, J. Power Sources 162 (2006) 1226–1231.
[27] A. Lewandowski, K. Skorupska, J. Malinska, Solid State Ionics 133 (2000) 265–271.
[28] Z. Peng, L.X. Kong, S.D. Li, Synt. Met. 152 (2005) 25–28.
[29] R.W. Berg, A.D. Otero, Vib. Spectrosc. 42 (2006) 222–225.
[30] A. Martinelli, A. Matic, P. Jacobsson, L. Borjesson, M.A. Navarra, A. Fernicola, S. Panero, B. Scrosati, Solid State Ionics 177 (2006) 2431–2435.